# Simple constitutive analysis of AA 7075-T6 aluminium alloy deformed at low deformation temperatures

**E. S. Puchi-Cabrera*[1,2,3], M. H. Staia[1], E. Ochoa-Pérez[1], J. G. La Barbera-Sosa[1], Y. Y. Santana[1], C. Villalobos-Gutiérrez[4] and J. R. Picón-Chaparro[1]**

The tensile stress–strain behaviour of AA 7075-T6 aluminium alloy deformed at temperatures in the range of 123–248 K, at strain rates between 0·0023 and 0·21 $s^{-1}$ has been analysed in order to develop a rational constitutive description of the material under such deformation conditions. The constitutive formulation has been derived on the basis of the mechanical threshold stress model developed at Los Alamos National Laboratory. The constitutive equation thus proposed is able to separate the contribution of the different components that give rise to the mechanical strength of the alloy. It has been determined that the flow stress of the material arises mainly from the contribution of three different components: athermal barriers to dislocation motion, solid solution and precipitation hardening and work hardening (dislocation–dislocation interaction). The flow stress in each strain increment during the course of plastic deformation is computed recursively from its previous value, before the updating of the deformation temperature and strain rate values. Such a computation is carried out by the numerical integration of the phenomenological work hardening law expressed in differential form. The constitutive description thus proposed provides an accurate prediction of the experimental values of both the flow stress and work hardening rate of the material. Moreover, its formulation in differential form provides a reasonable description of the stress changes that could take place when arbitrary temperatures and strain rate paths are imposed to the material during plastic deformation. It is shown that the formulation is general enough for describing also the constitutive behaviour and stress changes of a different aluminium alloy deformed under hot working conditions, where the material exhibits positive work hardening before achieving saturation at large strains.

**Keywords:** Constitutive description, AA 7075-T6 aluminium alloy, Low deformation temperatures

## List of symbols

$A$ material parameter
**b** Burgers vector/nm
$c_p$ heat capacity
$d\sigma_e/d\varepsilon$ work hardening rate/MPa
$e$ engineering strain
$g_0$ experimental normalised activation energy
$g_{0i}$ experimental normalised activation energy
$g_{0\dot{\varepsilon}s}$ experimental normalised activation energy
$k$ Boltzmann constant/J $K^{-1}$
$N$ number of experimental data points
$s$ engineering stress/MPa
$S$ $(T,\dot{\varepsilon})$ ratio between the current flow stress and the mechanical threshold stress or flow stress at 0 K
$T$ absolute temperature/K
$T_0$ initial specimen temperature/K

$\varepsilon$ effective strain
$\dot{\varepsilon}$ effective strain rate/$s^{-1}$
$\dot{\varepsilon}_K$ material parameter/$s^{-1}$
$\dot{\varepsilon}_{Ki}$ material parameter/$s^{-1}$
$\dot{\varepsilon}_{K\dot{\varepsilon}s}$ material parameter/$s^{-1}$
$\theta_0$ initial work hardening rate/MPa
$\mu$, $\mu$ $(T)$ temperature dependent shear modulus/GPa
$\mu_0$ shear modulus at 0 K/GPa
$\rho$ density/kg $m^{-3}$
$\sigma$ current flow stress/MPa
$\sigma_a$ athermal flow stress component/MPa

[1]School of Metallurgical Engineering and Materials Science, Faculty of Engineering, Universidad Central de Venezuela, Postal Address 47885, Los Chaguaramos, Caracas 1041, Venezuela
[2]Venezuelan National Academy for Engineering and Habitat, Palacio de las Academias, Postal Address 1723, Caracas 1010, Venezuela
[3]University Lille Nord de France, USTL, LML, CNRS, UMR 8107, F-59650 Villeneuve d'Ascq, France
[4]School of Mechanical Engineering, Faculty of Engineering, Universidad Central de Venezuela, Postal Address 47885, Los Chaguaramos, Caracas 1041, Venezuela

*Corresponding author, email epuchi@reacciun.ve


Published by Maney on behalf of the Institute
Received 2 March 2011; accepted 12 October 2011
DOI 10.1179/1743284711Y.0000000102

$\sigma$ $(T,\dot{\varepsilon})$ temperature and strain rate dependent flow stress/MPa
$\sigma_i$ $(T,\dot{\varepsilon})$ contribution of solid solution and precipitation hardening to the current flow stress/MPa
$\sigma_y$ $(T,\dot{\varepsilon})$ yield stress of the material/MPa
$\sigma_\varepsilon$ $(T,\dot{\varepsilon})$ contribution of work hardening to the current flow stress/MPa
$\sigma_{\varepsilon s}$ $(T,\dot{\varepsilon})$ temperature and strain rate dependent saturation stress/MPa
$\hat{\sigma}$ mechanical threshold stress or flow stress at 0 K/MPa
$\hat{\sigma}_i$ contribution of solid solution and precipitation hardening to the mechanical threshold stress or flow stress at 0 K/MPa
$\hat{\sigma}_{\varepsilon s}$ saturation stress at 0 K or mechanical threshold saturation stress/MPa
$\Omega$ objective function for minimisation/MPa$^2$

## Introduction

In the past 50 years, the aircraft industry has experienced a significant development, particularly in relation to airframe design and manufacturing processes. Such a development has been possible due to the manufacture of airframes with improved structural integrity, durability and damage tolerance characteristics. For this purpose, aluminium alloys with higher mechanical properties particularly in relation to fatigue and crack propagation resistance under constant amplitude and spectrum loading, as well as higher fracture toughness under plane stress and plane strain conditions and resistance to stress corrosion cracking, exfoliation and intergranular attack, have been required.

Aluminium alloys of the 7000 series, with a high Zn alloying content and supplied as sheet, plate and extrusion forms have been widely employed for the manufacture of different critical aircraft components which are subjected to compressive loads such as upper wing surfaces, internal ribs, spars, frames and landing gear. This has been accomplished through the development of different heat treatments to improve and optimise the balance between ultimate and yield strengths, ductility, resistance to the growth of fatigue cracks, toughness and resistance to corrosion.[1,2] However, further improvements in this sense require a better understanding and a rational procedure for determining and characterising the different microstructural mechanisms that contribute to the increase in the strength of these materials.

It is widely acknowledged that the mechanical strength of metals and alloys arises from the interaction of dislocations with different types of barriers intrinsic to the material. In general, such barriers to dislocation motion are classified in two broad groups: on the one hand, short range obstacles, also known as thermal barriers, such as Peierls–Nabarro forces, forest dislocations, solute atoms, small precipitates, etc., which can be overcome by dislocations with the assistance of thermal activation; on the other hand, long range obstacles or athermal barriers, such as grain boundaries, large precipitates, long range stress fields arising from dislocation pileups, etc., which dislocations cannot overcome by thermal activation.

The general theory of thermally activated plastic flow has been described in detail by different authors[3–5] and its results have been employed for expressing the constitutive behaviour of many different materials. In general, the correct constitutive description of a material should fulfil several important conditions. First, it should be formulated in terms of valid state parameters and therefore, the flow stress of the material should not be given as a function of strain but, for instance, in terms of dislocation density or any other valid structure parameter. This feature would allow for the possibility of strain path history effects. Second, it should distinguish the contribution of both athermal and thermal barriers to the flow stress and separate those contributions which are able to evolve in the course of plastic deformation from those which do not change. Third, the structure evolution should be expressed in differential form, which would be more useful for dealing with arbitrary strain rate and temperature paths.

One approach that fulfils all these characteristics and therefore could be employed to accomplish the constitutive description of metals and alloys in a wide range of temperatures and strain rates is the so called mechanical threshold stress (MTS) model. This formulation, whose equations are already well established, was originally developed at Los Alamos National Laboratory and it is based on one internal state variable called the MTS or flow stress at 0 K, which represents the microstructure of the material. Accordingly, the flow stress of the material at any temperature and strain rate (current flow stress) depends entirely on its current microstructure and therefore, any changes that take place in microstructure will give rise to the corresponding changes in the mechanical strength of the material.

Since both the flow stress of the material and the rate of microstructural evolution are considered a function of deformation temperature and strain rate, according to this model, the constitutive description should be composed of two different parts: a kinetic equation, which relates the flow stress to strain rate and deformation temperature and an evolution equation formulated in differential form, which is also expressed in terms of temperature and strain rate, and able to describe the microstructural evolution in the course of plastic deformation. This sound formulation has been successfully applied for describing the constitutive behaviour of both ferrous and non-ferrous pure metals and alloys deformed in a wide spectrum of temperatures and strain rates.[6–12]

In the past few years, a number of research works have been carried out in order to analyse the plastic deformation of different metals and alloys at low deformation temperatures. Most of these investigations have been conducted on steels[13–18] and relatively few on face centred cubic metals and their alloys.[19–21] Thus, the present investigation, which complements a previous study carried out on this subject,[21] has been conducted in order to formulate, on the basis of a simplified form of the MTS model, a constitutive description for the AA 7075-T6 aluminium alloy deformed in tension at temperatures in the range of 123–248 K, both under constant and variable crosshead speeds, leading to sudden increases in strain rate from $\sim 0{\cdot}0023$ to $0{\cdot}21\ s^{-1}$. Once the correct description of the changes in flow stress and work hardening rate of the material in the course of plastic deformation is accomplished, the formulation is further examined by modelling hypothetical arbitrary strain rate and temperature paths imposed to the material. The approach employed in

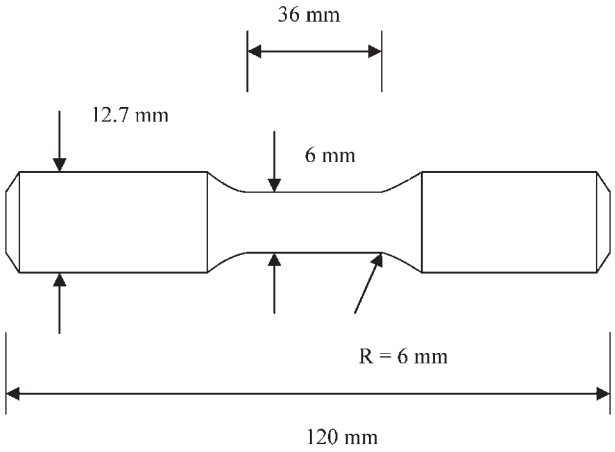


**1 Sketch of tensile samples employed in present investigation: measurements in mm**

this work represents an improvement of the formulation used in the previous investigation[21] and differs from it, not only in the magnitude and way in which the changes in crosshead speed were conducted, but also regarding the extension of the model to the analysis of the deformation of another aluminium alloy under hot working conditions.

## Experimental techniques

Tensile tests were carried out employing samples of AA 7075-T6 aluminium alloy, with the following chemical composition (wt-%): Al–6·10Zn–2·90Mg–2·00Cu–0·50Fe–0·40Si–0·30Mn–0·28Cr. The specimens were machined carefully according to the ASTM B557M-02a standard from bars of ~183 cm in length and 12·7 mm in diameter, in such a way as to avoid the introduction of flaws. However, SiC papers of 400–2000 grit were subsequently employed for the elimination of possible circumferential notches that could be introduced during their preparation. Figure 1 illustrates a sketch of the samples, where all the dimensions are given in mm.

The tests were carried out employing a computer controlled servohydraulic machine (model: AG-IS; 250 kN capacity; Shimadzu) equipped with a low temperature chamber. These were conducted at temperatures of 123, 173, 223 and 248 K, at both constant and variable crosshead speeds. Constant crosshead speed tests were carried out at 5, 50 and 500 mm $min^{-1}$; whereas, variable crosshead speeds tests involved the imposition of jumps from 5 to 50 and 5 to 500 mm $min^{-1}$. At least three samples were employed for each test condition. Given the dimensions of the specimens, the crosshead speeds employed in these experiments allowed the variation in the effective strain rate between ~0·0023 and 0·21 $s^{-1}$.

Effective strain, strain rate and stress data were obtained employing standard equations and when changes to a crosshead speed of 500 mm $min^{-1}$ took place, the nominal temperature of the specimen was corrected to take into consideration the deformational heating. Such a correction was carried out by means of the following relationship[6]

$$T = T_0 + \frac{0{\cdot}95}{\rho c_p}\int_0^e s(e)\mathrm{d}e \qquad (1)$$

where $T$ represents the corrected temperature, $T_0$ is the initial specimen temperature, $\rho$ is the density, $c_p$ is the heat capacity, $e$ is the engineering strain and $s(e)$ is the engineering stress.

## Results

Representative effective stress–strain curves obtained at different temperatures and crosshead speeds, either when this parameter was maintained constant or when jumps were imposed, are shown in Figs. 2–5. The experimental data are represented by means of continuous lines. The computed curves which result from the constitutive equation developed for this material are represented by means of small circles. Owing to the ductility of the alloy and nature of the tests (onset of necking), the maximum effective strains achieved in the tests varied between ~0·11 and 0·13. In this way, the framework of experimental conditions within which the constitutive description of the alloy has been formulated, is established. Although the range of strain rates and temperatures explored in this work could seem rather limited, it spans a wide spectrum of conditions of engineering applications of such a material.

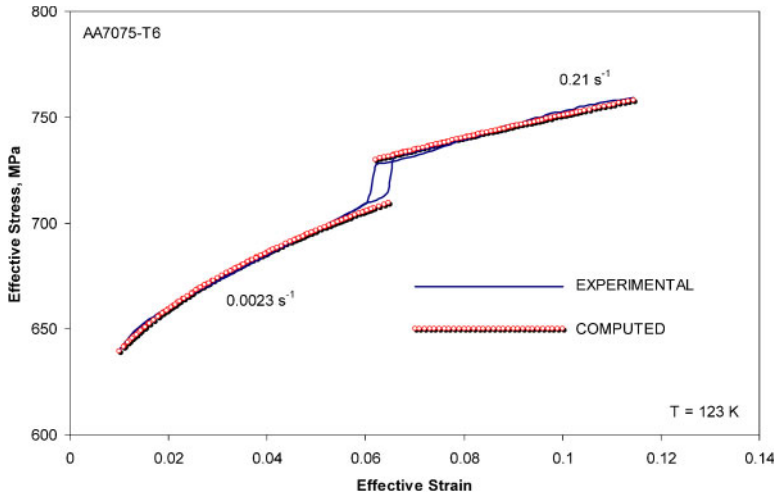


**2 Stress–strain curves obtained at 123 K: at strain of ~0·07, change in crosshead speed, leading to corresponding changes in strain rate from 0·0023 to 0·21 $s^{-1}$, has been conducted**

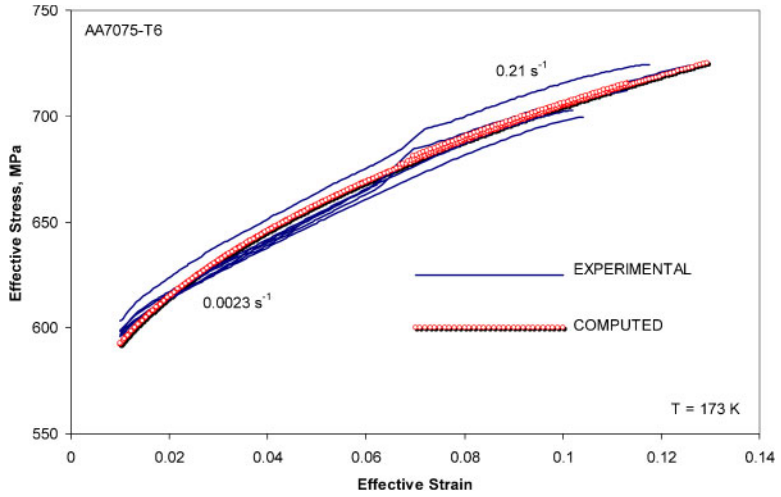


**3 Stress–strain curves obtained at 173 K: changes in crosshead speeds at strains of 0·06 and 0·07 are also shown**

In order to provide an idea of the reproducibility of the tests, Figs. 2–5 illustrate different stress–strain curves obtained under the same deformation conditions. As indicated above, some of the tests were conducted under conditions of constant crosshead speed and others under increasing crosshead speed. Therefore, since the strain interval over which the speed change occurs is very short, the computed stress–strain curves are represented by different branches, displaced from one to another.

Under the present deformation conditions, changes in strain rate have a minor effect on the flow stress of the material in comparison with changes in deformation temperature. As an example and as shown in Fig. 2, when the strain rate increases from 0·0023 to 0·21 $s^{-1}$ and the material is deformed at 123 K, the flow stress increases just in $\sim$16 MPa. On the contrary, as can be observed by comparing Figs. 2 with 5, when deformation temperature decreases from 248 to 123 K at a strain rate of 0·0023 $s^{-1}$, the flow stress at an effective strain of 0·045 increases in $\sim$74 MPa. As shown in Figs. 2–5, the reproducibility of the tensile tests conducted under constant conditions of deformation temperature and crosshead speed is quite satisfactory.

The analysis of the different components that contribute to the mechanical strength of the alloy has been carried out employing the concepts established in the MTS model. Particularly for this aluminium alloy, it has been considered that the strength arises from three different sources: athermal barriers, solid solution and precipitation strengthening and work hardening (dislocation–dislocation interactions). The first two components depend on deformation temperature and strain rate, but do not change in the course of plastic deformation. On the contrary, the last component (also dependent on temperature and strain rate) evolves in the course of plastic deformation. Thus, a plausible description of the flow stress of the material at any temperature and strain could be given by

$$\frac{\sigma(\hat{\sigma},T,\dot{\varepsilon})}{\mu(T)}=\frac{\sigma_a}{\mu(T)}+\frac{\sigma_i(\hat{\sigma}_i,T,\dot{\varepsilon})}{\mu_0}+\frac{\sigma_\varepsilon(\hat{\sigma}_\varepsilon,T,\dot{\varepsilon})}{\mu_0} \quad (2)$$

where $\hat{\sigma}$ represents the MST, $\sigma_a$ is the contribution of athermal barriers to the flow stress, $\mu(T)$ (MPa) is the temperature dependent shear modulus of the material, which is given by[9]

$$\mu(T)=28815-\frac{3440}{\exp(215/T)-1} \quad (3)$$

$\mu_0$ represents the shear modulus at 0 K (28 815 MPa), $\hat{\sigma}_i$ is the contribution of solid solution and precipitation hardening to the flow stress at 0 K, $\hat{\sigma}_\varepsilon$ ($\hat{\sigma}_\varepsilon$,$T$, $\dot{\varepsilon}$) is the

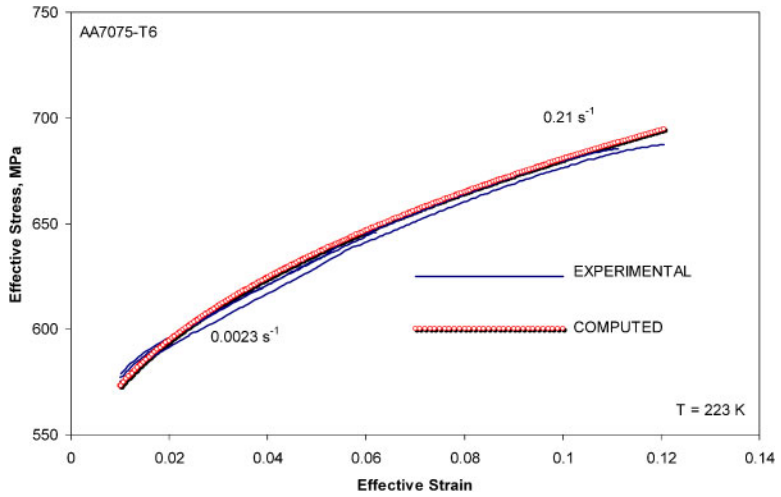


**4 Stress–strain curves obtained at 223 K: changes in crosshead speeds at strain of 0·06 are also shown**

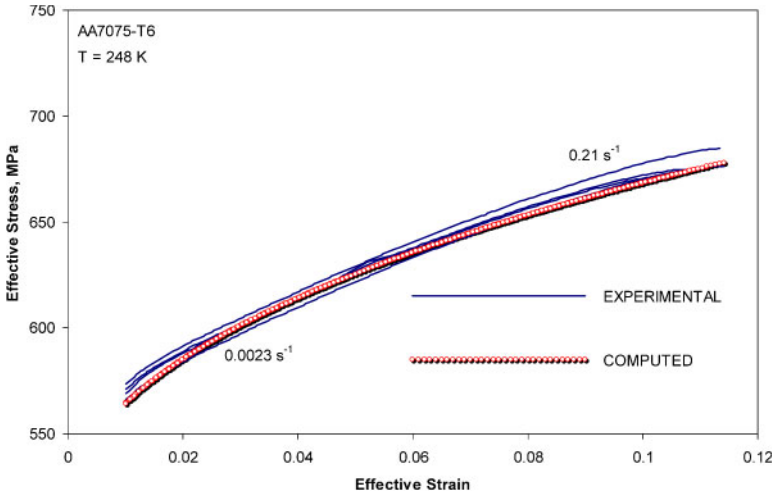


**5 Stress–strain curves obtained at 248 K: changes in crosshead speeds at strain of 0·05 are also shown**

contribution provided by work hardening to the flow stress also at 0 K; whereas, $\sigma_i$ and $\sigma_\varepsilon$ are the contribution of both mechanisms at any finite temperature and strain rate, $T$ is the absolute temperature and $\dot{\varepsilon}$ is the effective strain rate. In equation (2), the component $\sigma_\varepsilon$ appears expressed in terms of $\hat{\sigma}_\varepsilon$, a parameter that represents the microstructure of the material, rather than on strain, which is not a valid state parameter. Its computation should be carried out recursively from its previous value, by means of the numerical integration of the corresponding work hardening law employed in the formulation.

The component $\sigma_i$ can be expressed in terms of $\hat{\sigma}_i$, temperature and strain rate by means of an expression of the form[22]

$$\sigma_i\left(\hat{\sigma}_i,T,\dot{\varepsilon}\right)=\hat{\sigma}_i\left(\frac{\dot{\varepsilon}}{\dot{\varepsilon}_{Ki}}\right)^{\frac{kT}{g_{0i}\mu(T)\mathbf{b}^3}} \tag{4}$$

where $\dot{\varepsilon}_{Ki}$ represents a material constant, $k$ is the Boltzmann constant, $g_{0i}$ is a normalised activation energy and **b** is the Burgers vector (0·286 nm). The change in this parameter with deformation temperature can be introduced into the analysis by means of the linear expansion coefficient of the material ($26\times10^{-6}$ K$^{-1}$).

The evolution of the component $\hat{\sigma}_\varepsilon$ with plastic deformation has been described by means of the phenomenological work hardening law proposed by Estrin and Mecking[23]

$$\frac{d\hat{\sigma}_\varepsilon}{d\varepsilon}=\frac{\theta_0^2}{\hat{\sigma}_\varepsilon}\left[1-\left(\frac{\hat{\sigma}_\varepsilon}{\hat{\sigma}_{\varepsilon s}}\right)^2\right] \tag{5}$$

which is a modification of the Voce law[24,25] to account for dislocation motion in materials strengthened by particle dispersion or a fine grain size microstructure. In the above equation, $\theta_0$ represents the work hardening rate at zero stress and is given by

$$\theta_0=\frac{\mu(T)}{A} \tag{6}$$

where $A$ represents a material parameter and $\hat{\sigma}_{\varepsilon s}$ is the saturation threshold stress, i.e. the saturation stress of the material when it is hypothetically deformed at 0 K to large plastic strains.

The saturation stress of the material at any finite temperature and strain rate $\sigma_{\varepsilon s}(T,\dot{\varepsilon})$ can be obtained from $\hat{\sigma}_{\varepsilon s}$ by means of an extrapolation function of the form[22]

$$\sigma_{\varepsilon s}(T,\dot{\varepsilon})=\hat{\sigma}_{\varepsilon s}\left(\frac{\dot{\varepsilon}}{\dot{\varepsilon}_{K\varepsilon}}\right)^{\frac{kT}{g_{0\varepsilon}\mu(T)\mathbf{b}^3}} \tag{7}$$

where $\dot{\varepsilon}_{K\varepsilon}$ represents a material parameter and $g_{0\varepsilon}$ is a normalised activation energy.

The non-evolutive part of the flow stress, i.e. the yield stress of the material at any finite temperature and strain rate $\sigma_y(T,\dot{\varepsilon})$ can also be expressed according to equations (2) and (4) as

$$\frac{\sigma_y(T,\dot{\varepsilon})}{\mu(T)}=\frac{\sigma_a}{\mu(T)}+\frac{\hat{\sigma}_i}{\mu_0}\left(\frac{\dot{\varepsilon}}{\dot{\varepsilon}_{Ki}}\right)^{\frac{kT}{g_{0i}\mu\mathbf{b}^3}} \tag{8}$$

Thus, equation (5), together with the parameters $A$ (equation (6)), $\hat{\sigma}_{\varepsilon s}$ (equation (7)) and the constants $\sigma_a$ and $\hat{\sigma}_i$ (equation (8)), defines entirely the hypothetical stress–strain curve of the material at 0 K, i.e. the MTS.

Equations (2)–(8) represent the constitutive description of the material employed in the present work. These relationships encompass eight material parameters that should be computed simultaneously from the experimental strain, stress, strain rate and temperature data: $\sigma_a$ and $\hat{\sigma}_i$ (equation (2)), $\dot{\varepsilon}_{Ki}$, $\dot{\varepsilon}_{K\varepsilon}$ and $g_{0i}$ and $g_{0\varepsilon}$ (equation (4)), $\hat{\sigma}_{\varepsilon s}$ (equation (5)) and $A$ (equation (6)). However, the rational determination of these parameters should be carried out in two separate steps.

The first step implied the determination of a first approximation of the constants $\sigma_a/\mu$, $\hat{\sigma}_i$, $\dot{\varepsilon}_{Ki}$ and $g_{0i}$, employing approximate values of the yield stress of the material, normalised by the shear modulus, which were fitted to equation (8). Such constants were determined simultaneously by means of non-linear least square analysis and the results obtained are presented in Fig. 6. The preliminary values of such constants are given in Table 1. As shown in Fig. 6, equation (8) can describe quite satisfactorily the non-evolutive part of the flow stress. As previously indicated by Cerreta *et al.*,[12] the athermal component is only a function of temperature through the shear modulus.

As indicated above, the values of $\hat{\sigma}_\varepsilon$ are computed recursively, i.e. the current value of such a parameter is

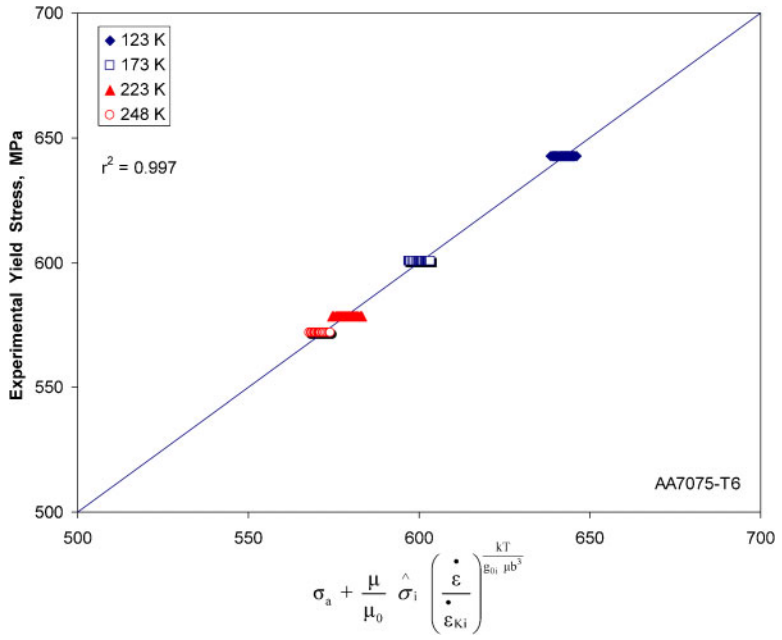


**6 Comparison between experimental and computed values of yield stress according to equation (8)**

calculated from its previous value, after updating the magnitude of the deformation temperature and strain rate corresponding to the current strain increment. In the present work, the numerical integration of equation (5) was carried out employing a fourth order Runge–Kutta scheme. In this way, the value of $\hat{\sigma}_{\varepsilon}$ at the end of each strain interval is computed in terms of the constants $\hat{\sigma}_{\varepsilon s0}$, $\dot{\varepsilon}_{K\varepsilon s}$, $g_{0\varepsilon s}$ and $A$, and the state variables $T$ and $\dot{\varepsilon}$. All the constants involved in the formulation are then determined simultaneously by defining the objective function

$$\Omega = \sum_{i=1}^{N} \left( \sigma_i^{\text{Computed}} - \sigma_i^{\text{Experimental}} \right)^2 \tag{9}$$

and solving simultaneously the set of equations that result from the minimisation condition

$$\begin{aligned} &\frac{\partial \Omega}{\partial (\sigma_a/\mu)} = 0; \quad \frac{\partial \Omega}{\partial \hat{\sigma}_i} = 0; \quad \frac{\partial \Omega}{\partial \dot{\varepsilon}_{Ki}} = 0; \quad \frac{\partial \Omega}{\partial g_{0i}} = 0 \\ &\frac{\partial \Omega}{\partial A} = 0; \quad \frac{\partial \Omega}{\partial \hat{\sigma}_{\varepsilon s}} = 0; \quad \frac{\partial \Omega}{\partial \dot{\varepsilon}_{K\varepsilon}} = 0; \quad \frac{\partial \Omega}{\partial g_{0\varepsilon}} = 0 \end{aligned} \tag{10}$$

In the present case, the solution of the above set of equations was carried out by means of the conjugate gradient method. Thus, Table 2 summarises the whole set of values of the constants involved in the proposed constitutive description for the investigated alloy.

**Table 1 Preliminary values of constants involved in equation (8)**

| $\sigma_a/\mu$/MPa | $\hat{\sigma}_i$/MPa | $\dot{\varepsilon}_{Ki}$/s$^{-1}$ | $g_{0i}$ |
|---|---|---|---|
| 0·022 | 510 | 107·8 | 0·024 |

As shown in Figs. 2–5, the computed curves employing the proposed constitutive description, together with the parameters determined from the experimental data, reproduce quite satisfactorily both the magnitude of the flow stress and the change in work hardening rate during the course of plastic deformation. In addition, as it is clearly illustrated in Fig. 2, the constitutive equation is able to predict quite accurately the change in flow stress when a sudden increase in crosshead speed and therefore in strain rate, occurs. The behaviour predicted by the constitutive description when arbitrary changes in deformation conditions take place will be discussed in more detail in the forthcoming.

A better illustration of the accuracy of the proposed constitutive description for predicting the flow stress values of the alloy is presented in Figs. 7 and 8. Figure 7 shows the comparison between the experimental and predicted values of the flow stress when the alloy is deformed at different temperatures and crosshead speeds. Thus, it can be clearly observed that the present constitutive equation reproduces quite accurately the flow stress values of the material in the range of temperatures and crosshead speeds examined. More precisely, Fig. 8 illustrates that the maximum relative error between the experimental and computed values of the flow stress is in general less than $\pm 2\%$, including the stress–strain curves where sudden changes in crosshead speed took place.

Thus, as far as this section is concerned, it can be concluded that the set of equations (2)–(8), which describe the constitutive formulation of the alloy and the numerical procedure employed for the determination of the constants involved in such relationships from the experimental data, lead to the development of a sound description of the change in flow stress in the course of

**Table 2 Parameters involved in constitutive formulation of AA 7075-T6 aluminium alloy**

| $\sigma_a/\mu$/MPa | $\hat{\sigma}_i$/MPa | $\dot{\varepsilon}_{Ki}$/s$^{-1}$ | $g_{0i}$ | $A$/MPa | $\hat{\sigma}_{\varepsilon s}$/MPa | $\dot{\varepsilon}_{K\varepsilon}$/s$^{-1}$ | $g_{0\varepsilon}$ |
|---|---|---|---|---|---|---|---|
| 0·019 | $1{\cdot}46 \times 10^4$ | $2{\cdot}58 \times 10^{13}$ | 0·016 | 65·2 | $1{\cdot}18 \times 10^4$ | 1·36 | 0·67 |

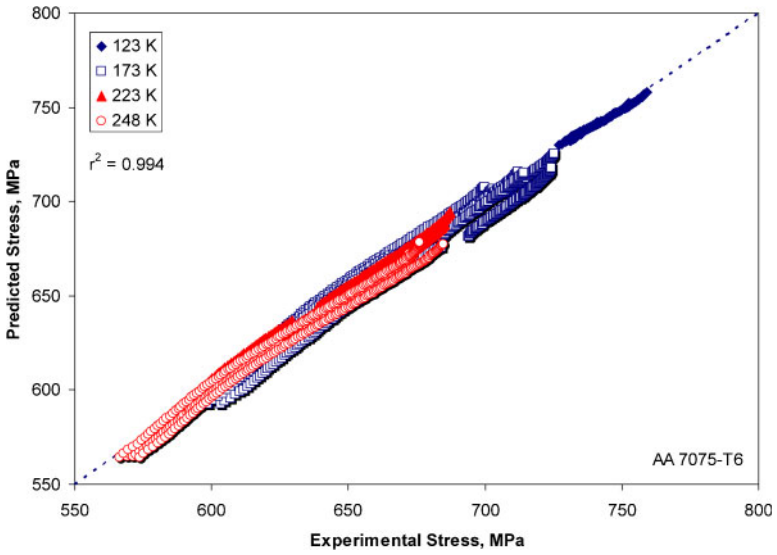


**7 Comparison between experimental and predicted values of flow stress, according to constitutive formulation of material**

plastic deformation for the alloy under investigation, at least in the range of experimental conditions that have been examined. However, additional aspects of the constitutive description such as the limitations to its applicability and ability to predict changes in flow stress when arbitrary changes in deformation conditions take place should be further discussed.

## Discussion

The constitutive description that has been developed on the basis of a simplified form of the MTS model fulfils all the basic aspects of a relationship of this nature that were indicated previously. First, it is able to separate the main components that contribute to the mechanical strength of the alloy under the present deformation conditions. Two of such components, namely the athermal stress and the interaction of dislocations with solute atoms and small precipitates constitute the non-evolutive part of the flow stress. The third component, namely the interaction of dislocation with other dislocations constitutes the evolutive part of the flow stress. Thus, under the present conditions, the strength of the alloy can be considered to arise from the contribution of these three components. However, the observation of the experimental flow stress curves indicates that in the range of deformation temperatures and strain rates employed in the present investigation, the yield stress of the material represents a significant contribution of the overall alloy strength. As expected, as plastic deformation takes place, work hardening also starts contributing to the strength of the material and the extent of such contribution increases as deformation temperature decreases and strain rate increases.

Second, the constitutive description given in this form reproduces quite accurately the values of the flow stress and therefore represents an accurate and reliable relationship for the computation of the mechanical strength of the alloy under the investigated conditions. Moreover, the number of material parameters involved in the description is relatively small, given the detailed account of the involvement of the different components that contribute to the flow stress of the alloy.

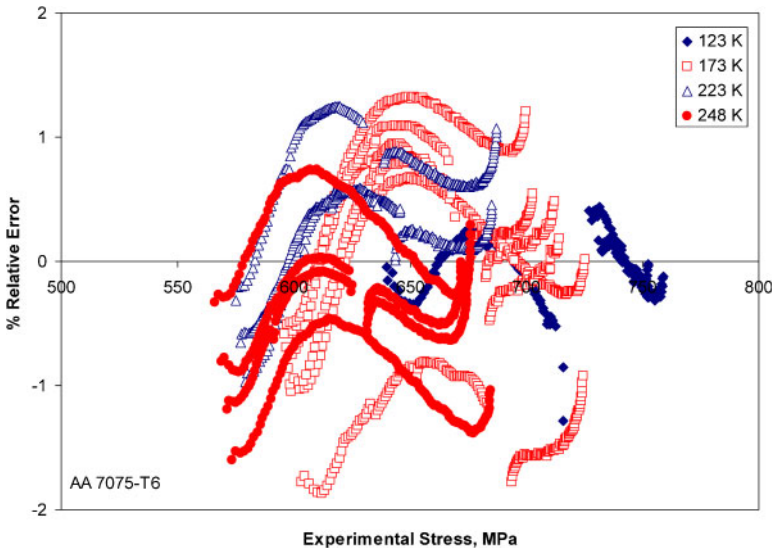


**8 Change in relative error between experimental and predicted values of flow stress as function of former**

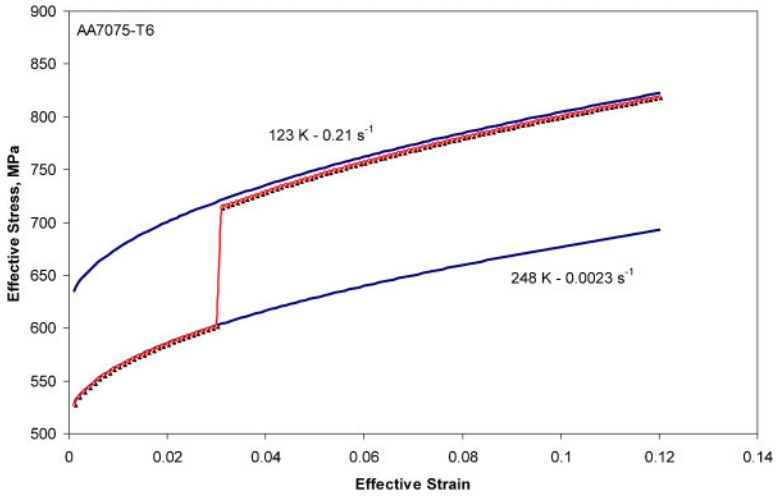


**9 Hypothetical change in deformation conditions that could occur by first deforming material at temperature of 248 K at strain rate of 0·0023 $s^{-1}$ and suddenly, changing conditions to deformation temperature of 123 K at strain rate of 0·21 $s^{-1}$, at effective strain of 0·03**

However, one of the main limitations of the present description is the fact that the flow stress curves were determined under tensile conditions. Therefore, the maximum strain achieved in the tests is imposed by the onset of necking, which in the present case occurred at effective strains in the range of $\sim$0·12. Such a limitation could be overcome by conducting compression tests, by means of which larger homogeneous strains can be achieved, once the friction effects are appropriately corrected. A second limitation of the present constitutive description is the upper deformation temperature of the material which would be determined by the aging temperature of the alloy ($\sim$120°C), at which the precipitation hardening component of the flow stress could be significantly altered.

Regarding the extrapolation of the hardening components $\hat{\sigma}_i$ and $\hat{\sigma}_{\varepsilon s}$ of the MTS to finite temperatures and strain rates, the most satisfactory outcome was obtained by employing equations (4) and (7) respectively, together with the evolution law described in equation (5). Such relationships are somewhat different from those employed in the actual MTS model, but as shown in Figs. 6–8, these are able to provide the correct description of the temperature and strain rate dependence of the yield stress and the flow stress, in general.

A final feature that should be discussed in relation to the proposed constitutive description is its capability for describing hypothetical arbitrary changes in deformation conditions. Although Fig. 2 illustrates already the ability of the constitutive equation for describing the change in flow stress that occurs when the strain rate is suddenly increased from $\sim$0·0023 to 0·21 $s^{-1}$, it would be important to examine the predictions of the equation when other hypothetical arbitrary changes in deformation conditions take place.

The formulation of the constitutive description of the material in differential form and the computation of the flow stress by means of the numerical integration of the corresponding work hardening law, as described in the preceding section, allows the updating of the deformation temperature and strain rate values in each strain increment. This feature cannot be accomplished when the flow stress of the material is expressed as a function of the applied strain in the form of an integrated equation.

Thus, the description of the flow stress of the material by means of an equation of the form $\sigma = f(\varepsilon, \dot{\varepsilon}, T)$

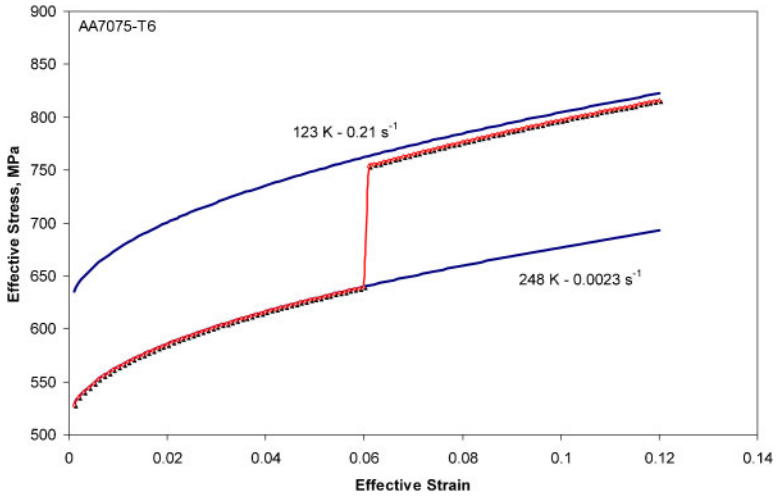


**10 Hypothetical change in deformation conditions that could occur by first deforming material at temperature of 248 K at strain rate of 0·0023 $s^{-1}$ and suddenly, changing conditions to deformation temperature of 123 K at strain rate of 0·21 $s^{-1}$, at effective strain of 0·06**

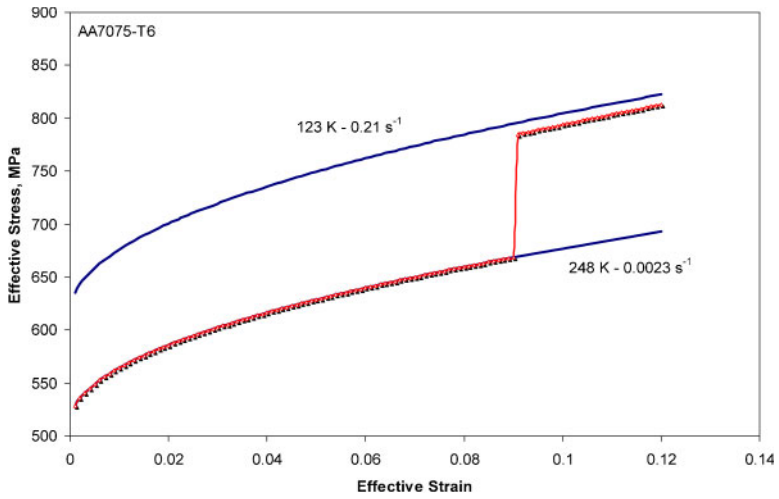


**11 Hypothetical change in deformation conditions that could occur by first deforming material at temperature of 248 K at strain rate of 0·0023 $s^{-1}$ and suddenly, changing conditions to deformation temperature of 123 K at strain rate of 0·21 $s^{-1}$, at effective strain of 0·09**

assumes the validity of an equation of state and therefore is unable to describe the changes in flow stress that take place under variable deformation conditions. On the contrary, when the flow stress is computed recursively by the numerical integration of the work hardening law, such changes can be described in a precise manner depending on the accuracy of the constitutive equation, as shown in Figs. 9–11. These figures illustrate hypothetical and arbitrary instantaneous changes in deformation conditions, from a deformation temperature of 248 K and a strain rate of 0·0023 $s^{-1}$, to a temperature of 123 K and a strain rate of 0·21 $s^{-1}$, at three different strains.

In each case, the jump that occurs in flow stress does not achieve the upper flow stress curve, as it would be predicted by a mechanical equation of state. On the contrary, the value attained is less than that corresponding to the flow stress at the particular strain where the change occurred and a subsequent evolution takes place during which the flow stress approaches the upper curve. Thus, the sudden increase in flow stress is associated with the non-evolutive part of the flow stress. Moreover, the above figures indicate that as the strain at which the change in deformation conditions occurs increases, the strain transient required for the flow stress to achieve the upper flow curve also increases.

A similar behaviour is observed in Figs. 12–14 which show changes in deformation conditions but in the opposite direction, i.e. from 123 K and 0·21 $s^{-1}$ to 248 K and 0·0023 $s^{-1}$. Again, it can be observed that when the change takes place, the flow stress does not achieve instantaneously the stress value that corresponds to the lower curve, but a higher one. It is only after a strain transient whose magnitude depends on the strain at which the change took place that the flow stress approaches the lower flow stress curve.

The shape of the flow curve during the strain transient depends significantly on the work hardening characteristics of the material and the ability of dynamic recovery to counteract the increase in flow stress due to work hardening. However, under the present deformation conditions, dynamic recovery processes are severely restricted due to the low deformation temperatures at which plastic deformation occurs and therefore the

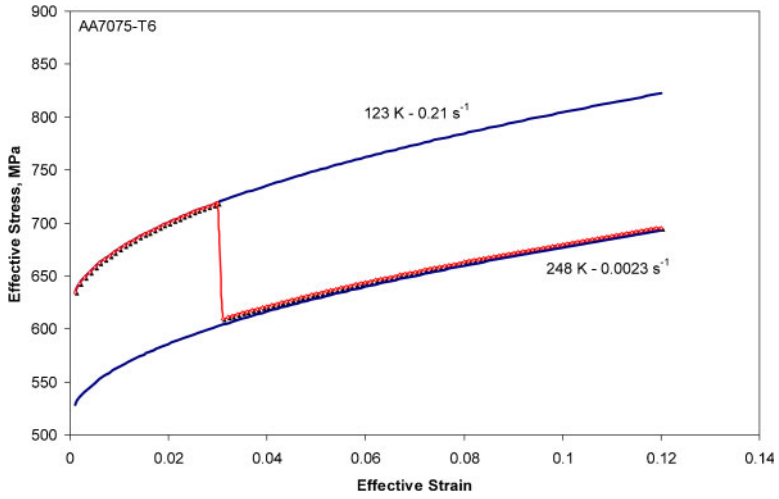


**12 Hypothetical change in deformation conditions that could occur by first deforming material at temperature of 123 K at strain rate of 0·21 $s^{-1}$ and suddenly, changing conditions to deformation temperature of 248 K at strain rate of 0·0023 $s^{-1}$, at effective strain of 0·03**

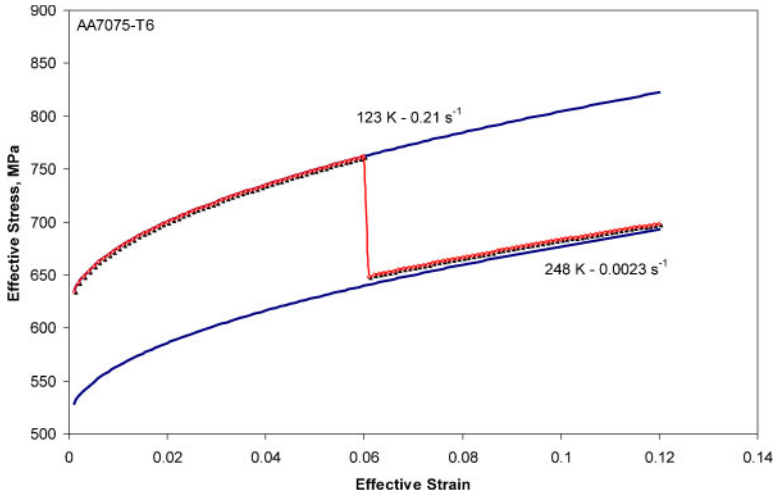


**13 Hypothetical change in deformation conditions that could occur by first deforming material at temperature of 123 K at strain rate of 0·21 $s^{-1}$ and suddenly, changing conditions to deformation temperature of 248 K at strain rate of 0·0023 $s^{-1}$, at effective strain of 0·06**

changes in the dislocation substructure in order to achieve the configuration corresponding to the final deformation conditions are very slow.

The present constitutive analysis has also been extended to describe the changes that take place in flow stress with deformation conditions when an Al–1Mg alloy is deformed under hot working conditions, employing experimental data reported elsewhere.[26] The results of this analysis are shown in Figs. 15 and 16, making use of the appropriate set of constants for this material. Particularly, Fig. 16 illustrates two hypothetical changes in deformation conditions and the predictions provided by the present constitutive equation. In this case, after the change takes place, the flow stress achieves the level corresponding to the final deformation condition following a stress transient. Therefore, the last two figures show clearly that the present constitutive description not only is able to describe correctly the change in flow stress with the strain applied when the material is deformed at different temperatures and strain rates. Also, these figures show that the hypothetical transients in flow stress when significant changes in deformation conditions occur are also predicted in a correct manner.

The possibility of updating the deformation temperature and strain rate in each strain increment throughout the course of plastic deformation has important practical implications, particularly in relation to the data derived from different mechanical tests. For instance, when tests are carried out under constant crosshead speed conditions, as in the present investigation, the strain rate changes continuously during deformation. In addition, depending on deformation conditions, deformational heating of the sample could be important, leading to a continuous increase in deformation temperature. The formulation of the constitutive equation in differential form does not require a prior temperature and strain rate iterative correction of the flow stress data before deriving the constitutive equation of the material since both parameters can be updated in each strain increment. On the contrary, when the flow stress is expressed explicitly as a function of the strain applied to the material in the form of an integrated equation, such updating is not possible

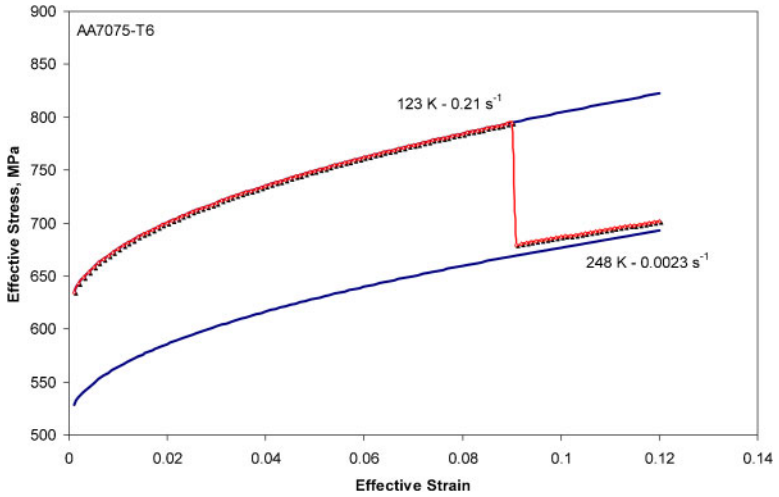


**14 Hypothetical change in deformation conditions that could occur by first deforming material at temperature of 123 K at strain rate of 0·21 $s^{-1}$ and suddenly, changing conditions to deformation temperature of 248 K at strain rate of 0·0023 $s^{-1}$, at effective strain of 0·09**

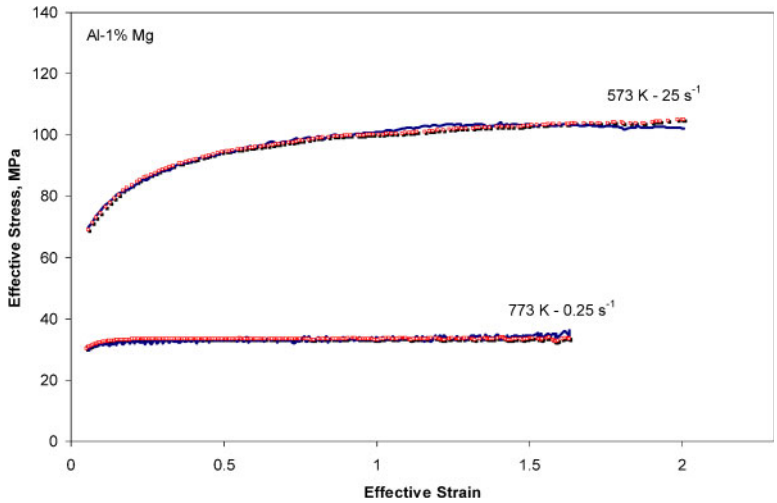


**15 Experimental and predicted stress–strain curves for Al–1Mg alloy deformed under hot working conditions: experimental curves have been reported elsewhere;[26] predicted curves were determined employing same formulation used for AA 7075-T6 aluminium alloy, with appropriate constants**

and therefore an iterative corrective procedure of the flow stress is required.

In summary, the present constitutive formulation has important advantages in comparison with the approaches that express the flow stress by means of integrated equations, particularly regarding the possibility of employing flow stress data obtained under variable conditions of deformation temperature and strain rate and also describing the flow stress transients that could occur when deformation conditions follow arbitrary temperature and strain rate paths, as those examined in the present work. Moreover, the procedure that has been described for its development is general enough to be employed in the determination of the constitutive description of other alloys deformed at different temperatures and strain rates, provided that the material exhibits positive work hardening.

## Conclusions

A constitutive description able to distinguish the contribution of different hardening components to the mechanical strength of AA 7075-T6 aluminium alloy deformed at low temperatures has been developed. The formulation represents a simplified approach of the MTS model developed at Los Alamos National Laboratory. Accordingly, the strength of the alloy during plastic deformation is considered to arise mainly from three different components: athermal barriers to dislocation motion, solid solution and precipitation hardening and work hardening. The contribution provided by solid solution and precipitation hardening does not evolve in the course of plastic deformation; whereas, work hardening is considered the only evolutionary component of the flow stress. The work hardening rate has been described by means of the phenomenological law proposed by Estrin and Mecking[23] and the flow stress is computed recursively by the numerical integration of such differential equation. The contributions of solid solution and precipitation hardening at 0 K, as well as that of the saturation threshold stress have been extrapolated to finite temperatures and strain rates by means of the model earlier advanced by Kocks.[22] It has been shown that the flow stress and work hardening rate of the material can be satisfactorily described by means of the

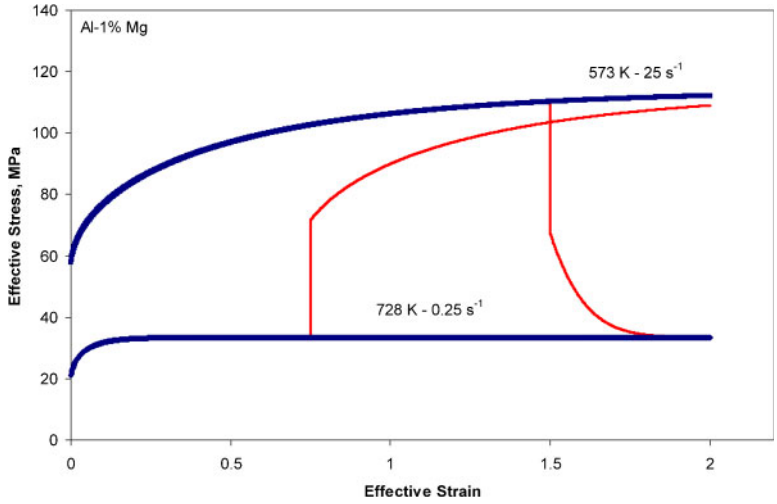


**16 Hypothetical changes in flow stress associated with sudden changes in deformation conditions under hot working conditions predicted by proposed constitutive description**

formulation thus developed. Moreover, the constitutive description is able to predict in a correct manner the occurrence of stress transients under different deformation conditions, when arbitrary paths in deformation temperature and strain rate take place. The differential formulation of the evolutive component of the flow stress allows the updating of the deformation temperature and strain rate in each strain increment and therefore, precludes the iterative correction of the flow stress before the development of the constitutive equation.

## Acknowledgement

The present investigation has been conducted with the financial support of the Scientific and Humanistic Development Council of the Universidad Central de Venezuela (CDCH-UCV) through the project PG-08-7775-2009/1. Professor Puchi-Cabrera gratefully acknowledges the financial support of the Conseil Régional Nord - Pas de Calais, France, through the International Chair program 2011.

## References

1. B. Cantor, H. Assender and P. Grant (eds.): 'Aerospace materials'; 2001, Bristol, Institute of Physics Publishing Ltd.
2. J. G. Kaufman: 'Introduction to aluminum alloys and tempers'; 2000, Materials Park, OH, ASM International.
3. H. Conrad: *J. Iron Steel Inst.*, 1961, **198**, 364–375.
4. H. Conrad: 'High-strength materials', Proc. 2nd Berkeley Int. Materials Conf., (ed. V. F. Zackay), 436–509; 1964, New York, John Wiley & Sons, Inc.
5. U. F. Kocks, A. S. Argon and M. F. Ashby: 'Thermodynamics and kinetics of slip'; 1975, New York, Pergamon Press.
6. P. S. Follansbee and U. F. Kocks: *Acta Metall.*, 1988, **36**, (1), 81–93.
7. P. S. Follansbee and G. T. Gray, III: *Metall. Trans. A*, 1989, **20A**, 863–874.
8. S. R. Chen and G. T. Gray, III: *Metall. Mater. Trans. A*, 1996, **27A**, 2994–3006.
9. S. R. Chen, M. G. Stout, U. F. Kocks, S. R. MacEwen and A. J. Beaudoin: in 'Hot deformation of aluminum alloys II', (ed. T. R. Bieler *et al.*), 205–216; 1998, Warrendale, PA, TMS.
10. G. T. Gray, III, S. R. Chen and K. S. Vecchio: *Metall. Mater. Trans. A*, 1999, **30A**, 1235–1247.
11. M. L. Newman, B. J. Robinson, H. Sehiteglu and J. A. Dantzig: *Metall. Mater. Trans. A*, 2003, **34A**, 1483–1491.
12. E. Cerreta, G. T. Gray, III, S. R. Chen and T. M. Pollock: *Mater. Trans. A*, 2004, **35A**, 2557–2566.
13. Y. Tomita: *Mater. Sci. Technol.*, 1988, **4**, (7), 613–620.
14. J. R. Buckley and D. Hardie: *Mater. Sci. Technol.*, 1993, **9**, (3), 259–263.
15. Y. Tomita: *Mater. Sci. Technol.*, 1995, **11**, (4), 335–340.
16. S. Xu, R. Bouchard and W. R. Tyson: *Metall. Mater. Trans. A*, 2004, **35A**, 1410–1414.
17. K. Spencer, M. Véron, K. Yu-Zhang and J. D. Embury: *Mater. Sci. Technol.*, 2009, **25**, (1), 7–17.
18. K. Spencer, M. Véron, K. Yu-Zhang and J. D. Embury: *Mater. Sci. Technol.*, 2009, **25**, (1), 18–22.
19. A. Molinary and G. Ravichandran: *Mech. Mater.*, 2005, **37**, 737–752.
20. G. Z. Voyiadjis and A. H. Almasri: *Mech. Mater.*, 2008, **40**, 549–563.
21. E. S. Puchi-Cabrera, M. H. Staia, E. Ochoa-Pérez, J. G. la Barbera-Sosa, C. Villalobos-Gutierrez and A. Brenlla-Caires: *Mater. Sci. Eng. A*, 2011, **A528**, 895–905.
22. U. F. Kocks: *J. Eng. Mater. Technol.*, 1976, **98**, 76–85.
23. Y. Estrin and H. Mecking: *Acta Metall.*, 1984, **32**, (1), 57–70.
24. E. Voce: *J. Inst. Met.*, 1948, **74**, 537–562.
25. E. Voce: *Metallurgia*, 1955, **51**, 219–226.
26. E. S. Puchi-Cabrera: *J. Eng. Mater. Technol.*, 2001, **123**, (3), 301–308.